Design of a Compact Biaxial Tensile Stage for Fabrication and Tuning of Complex Micro- and Nano-scale Wrinkle Patterns

Sourabh K. Saha[1]
Laboratory for Manufacturing and Productivity,
Department of Mechanical Engineering,
Massachusetts Institute of Technology,
Cambridge, MA 02139
e-mail: sourabh@alum.mit.edu

Martin L. Culpepper[2]
Laboratory for Manufacturing and Productivity,
Department of Mechanical Engineering,
Massachusetts Institute of Technology,
Cambridge, MA 02139
e-mail: culpepper@mit.edu

Wrinkling of thin films is a strain-driven process that enables scalable and low-cost fabrication of periodic micro- and nano-scale patterns. In the past, single-period sinusoidal wrinkles have been applied for thin-film metrology and microfluidics applications. However, real-world adoption of this process beyond these specific applications is limited by the inability to predictively fabricate a variety of complex functional patterns. This is primarily due to the inability of current tools and techniques to provide the means for applying large, accurate, and nonequal biaxial strains. For example, the existing biaxial tensile stages are inappropriate because they are too large to fit within the vacuum chambers that are required for thin-film deposition/growth during wrinkling. Herein, we have designed a compact biaxial tensile stage that enables (i) applying large and accurate strains to elastomeric films and (ii) in situ visualization of wrinkle formation. This stage enables one to stretch a 37.5 mm long film by 33.5% with a strain resolution of 0.027% and maintains a registration accuracy of 7 μm over repeated registrations of the stage to a custom-assembled vision system. Herein, we also demonstrate the utility of the stage in (i) studying the wrinkling process and (ii) fabricating complex wrinkled patterns that are inaccessible via other techniques. Specifically, we demonstrate that (i) spatial nonuniformity in the patterns is limited to 6.5%, (ii) one-dimensional (1D) single-period wrinkles of nominal period 2.3 μm transition into the period-doubled mode when the compressive strain due to prestretch release of plasma-oxidized polydimethylsiloxane (PDMS) film exceeds ~18%, and (iii) asymmetric two-dimensional (2D) wrinkles can be fabricated by tuning the strain state and/or the actuation path, i.e., the strain history. Thus, this tensile stage opens up the design space for fabricating and tuning complex wrinkled patterns and enables extracting empirical process knowledge via in situ visualization of wrinkle formation. [DOI: 10.1115/1.4031382]

Keywords: stretch release, period doubling, asymmetric wrinkles, strain history, path dependence

1 Introduction

Wrinkling is a strain-driven self-organization phenomenon that is commonly observed in natural systems over a wide length scale [1–3]. Recently, this phenomenon has been incorporated into engineered systems to generate micro- and nano-scale patterns [4,5]. For example, wrinkling of bilayer materials has been used to fabricate periodic sinusoidal patterns for thin-film metrology [5–7], stretchable electronics [8,9], and microfluidics applications [5,10]. Due to its inherent affordability and manufacturing scalability, pattern generation via wrinkling is an attractive potential alternative to more expensive cleanroom-based techniques such as e-beam lithography. However, practical import of this process is limited by the lack of flexibility, i.e., due to the inability to fabricate a variety of complex 2D patterns. This is due to the limited ability of current tools and techniques to provide *large*, *accurate*, *and/or nonequibiaxial strains* during wrinkling. Herein, we present the design of a compact biaxial tensile stage and demonstrate its utility in (i) exploring and accessing a wider design space for patterning and (ii) fabrication of tunable complex wrinkled patterns.

Wrinkles in compressed bilayer systems are formed due to buckling-based instabilities. The mechanism of wrinkling is similar to Euler buckling of columns under compression [11]. A schematic of the process is illustrated in Fig. 1. Essential elements of these bilayer systems are: (i) a film that is *thin* relative to the base, (ii) mismatch in the elastic moduli of the film and the base with the film being stiffer than the base, and (iii) loading conditions that generate in-plane compressive strain in the film. In such systems, the state of pure compression becomes unstable beyond a critical strain and wrinkles are formed via periodic bending of the film/base. The period of wrinkles is determined by the competing dependence of strain energy on period in the film versus in the base. Several different techniques have been developed in the past

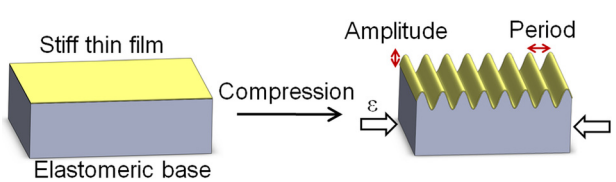

Fig. 1 Schematic of wrinkle formation via compression of a bilayer film

[1]Present address: Materials Engineering Division, Lawrence Livermore National Laboratory, P.O. Box 808, L-781, Livermore, CA 94551.
[2]Corresponding author.
Contributed by the Manufacturing Engineering Division of ASME for publication in the Journal of Micro- and Nano-Manufacturing. Manuscript received December 23, 2014; final manuscript received August 18, 2015; published online September 14, 2015. Assoc. Editor: Stefan Dimov.

to (i) generate and join/bond the film to the base [12–14], (ii) generate moduli mismatch [12,15–17], and (iii) apply uniaxial [6,12,13] and equibiaxial strains [14,18–20] to the film. Analytical and computational predictive models for uniaxial [11,21] and equibiaxial strains [22] have also been developed. As such, these techniques and models provide a framework for performing predictive design and fabrication of periodic wrinkle patterns.

Although the current techniques and models are a valuable toolkit for predictive design and fabrication of wrinkled patterns, they are still inadequate in satisfying the need for a variety of different complex patterns. This is primarily because only a small subset of the feasible design space is accessible via existing experimental techniques. The set of wrinkle patterns that can be fabricated is limited by the achievable range and types of compressive strains. For example: (i) below a threshold strain, only the single-period sinusoidal mode can be achieved via uniaxial strains [13] and (ii) only a limited set of symmetric 2D modes can be achieved via equibiaxial strains [22]. Existing techniques that rely on thermal expansion [14,20] or volumetric swelling [18,19] to generate strains can provide only a limited set of strain states. For example, mismatched thermal expansion of an isotropic film on an isotropic base generates equibiaxial strains. Due to this, exploring the design space for large uniaxial or nonequibiaxial strains becomes a material selection problem. This coupling between strain and materials can be eliminated by using mechanical stages to introduce strains via stretching of the base layer. However, the existing biaxial mechanical stages are often too large to use within vacuum chamber-based equipment that are necessary for generation of thin films during wrinkle fabrication. Thus, there is a need to develop a mechanical stage that has a small form factor and provides the means to apply large, accurate, and nonequibiaxial strains.

Compact mechanical stages that are capable of providing large nonequibiaxial strains become a necessity when a variety of complex wrinkle patterns are required. Herein, we present such a mechanical stage and demonstrate its capability to enable fabrication of tunable complex wrinkled patterns. Also, we (i) link the functional requirements for fabricating wrinkles to the design parameters of the stage, (ii) demonstrate the design and fabrication of the stage, (iii) characterize its performance, and (iv) demonstrate the fabrication and tuning of a set of complex wrinkle patterns. The stage is compact and is capable of providing uniaxial and sequential nonequibiaxial stretching. The stage also has features that enable one to register it to a vision system. This enables performing real-time in situ visualization of the wrinkles as stretches are varied. Thus, this system is an effective tool to (i) expand and explore the design space, (ii) investigate the tunability of patterns as stretches are varied, and (iii) fabricate the desired complex patterns.

2 Background and Functional Requirements

2.1 Fabrication of Wrinkle Patterns

2.1.1 Process Parameters. Wrinkling of compressed bilayers is an affordable fabrication technique for generating 1D periodic micro- and nano-scale patterns. The period and amplitude of these patterns can be tuned by controlling the relevant process parameters. For a bilayer system, these parameters are: (i) thickness of the top layer, (ii) compressive strain in the top layer, and (iii) ratio of stiffness moduli of the top and the bottom layers. Several analytical models for 1D wrinkling of bilayer systems are available in the literature. These models differ in terms of small strain [11,12] versus large strain [21] and linear [11,12] versus nonlinear material models [21,23]. For linear elastic materials at low uniaxial compressive strains, the period (λ) and amplitude (A) of the wrinkles may be estimated in terms of the top stiff layer thickness (h) as [12]

$$\lambda = 2\pi h \eta^{1/3} \tag{1}$$

$$A = \frac{\lambda}{\pi}(\varepsilon - \varepsilon_c)^{1/2} \tag{2}$$

Here, η is a nondimensional ratio of material properties, ε is the applied compressive strain, and ε_c is the critical strain above which wrinkles are observed. The critical strain is determined entirely by the material properties and is given by [12]

$$\varepsilon_c = -\frac{1}{4}\eta^{-2/3} \tag{3}$$

The material property ratio η in terms of the Young's moduli ($E_{f,s}$) and Poisson's ratio ($\nu_{f,s}$) of the top film and the bottom layer is given by [12]

$$\eta = \left(\frac{E_f}{3E_s}\right)\left(\frac{1-\nu_s^2}{1-\nu_f^2}\right) \tag{4}$$

Here, the subscripts f and s refer to the film and the base substrate, respectively. This simplified model captures the essential features of the wrinkling process: (i) length scale for the system is set by the thickness of the top film, (ii) effect of material properties is through the ratio of mechanical properties of the top and bottom layers, and (iii) amplitude of wrinkles can be tuned by varying the applied strain without affecting the period. Thus, to fabricate the desired wrinkle patterns, one must be able to tune and/or control these three parameters: top film thickness, material properties, and compressive strain. Typically, the top film thickness varies in the range of 10–100 nm, the ratio of layer stiffness moduli varies in the range of 10^3–10^5, and the compressive strain varies from 3% to 15%.

2.1.2 Process Steps and Equipment. To enable the fabrication and tuning of wrinkle patterns, one must solve these subproblems: (i) fabrication of a bilayer system with the desired material properties and geometry, (ii) compression of the top stiff film, and (iii) in situ visualization of pattern formation. Herein, we summarize the process steps and equipment that solve these subproblems, and then, in Sec. 2.3 we link the overall process/equipment goals to the functional requirements for designing the tensile stage.

2.1.2.1 Fabrication of bilayers. Stretchable bilayers with large stiffness ratio can be fabricated by attaching or growing a thin stiff film on top of a thick elastomeric base. For example, exposing a PDMS film to air or oxygen plasma leads to the formation of a thin glassy layer on top of the exposed PDMS surface via oxidation [20]. Alternatively, a metallic [14,24,25] or polymeric [26,27] thin film may be deposited on top of PDMS to obtain the desired bilayer. The top layer thickness can be tuned by controlling the duration of plasma oxidation or the deposition process; whereas the stiffness ratio may be tuned by selecting the appropriate top/bottom materials. Herein, we have used both air plasma oxidation and metal deposition to generate a stiff thin film on top of an elastomeric PDMS layer.

2.1.2.2 Compression of thin film. Compression of the top film can be achieved by either directly compressing the bilayer or by generating a residual compressive strain in the top layer. As direct compression requires sustained loading to maintain the wrinkles, the generation of residual compressive strain is often the preferred scheme. During mechanical loading, residual compression can be generated by first stretching the PDMS base and then attaching/growing the stiff film on top of this prestretched base layer. On releasing the prestretch in the PDMS, the top layer undergoes compression that leads to formation of wrinkles. Herein, we have exclusively used this prestretch-based technique to generate compressive strains in the thin film.

2.1.2.3 Process steps. The steps of the fabrication process are summarized in Fig. 2. The steps are: (i) fabricating the base PDMS film, (ii) clamping the PDMS film in the tensile stage, (iii)

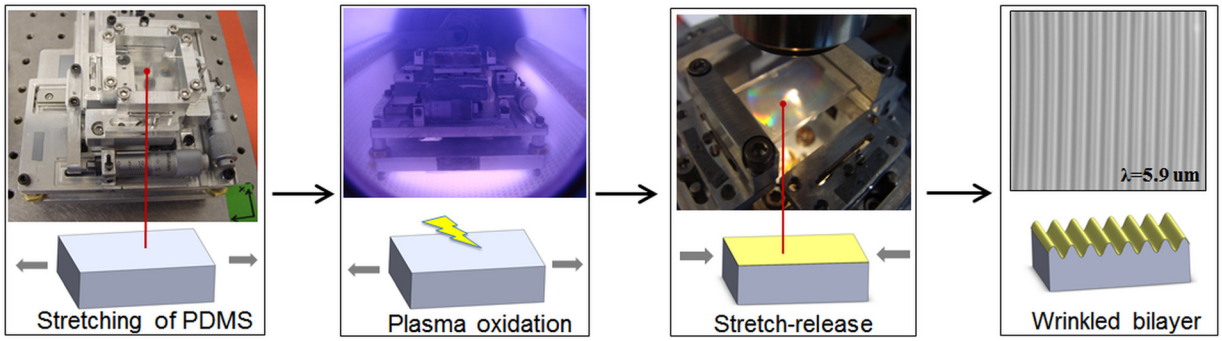

Fig. 2 Sequence of process steps and the equipment used in fabrication of wrinkle patterns

extension of the PDMS film, (iv) plasma oxidation of the stretched PDMS film or deposition of metallic thin film, and (v) release of the prestretch in the PDMS film. The role of the tensile stage is to provide the means to (i) control the stretch in the PDMS base layer, (ii) hold the prestretch during plasma oxidation or metal deposition, and (iii) perform a controlled release of the prestretch. Additionally, the stage must have alignment features to register itself to a vision system both before and after plasma oxidation to enable in situ visualization of wrinkle formation. The stage presented here satisfies all of these requirements.

2.2 Tuning of Wrinkle Patterns Via Strain. The morphology of wrinkles depends on both the magnitude and the nature of compressive strains that are applied to the thin film. The nature of the applied strain can be classified into three different types: (i) equibiaxial, (ii) uniaxial, and (iii) sequential biaxial. The application of equibiaxial strain leads to 2D periodic morphologies such as triangular, hexagonal, square checkerboard, and zigzag modes [22] whereas the application of uniaxial strain leads to 1D sinusoidal patterns [12]. For both of these types of strains, the morphology of wrinkles also changes when the compressive strain is progressively increased. During uniaxial loading, this change occurs as a transition from a single-period sinusoidal mode to higher modes of successive period-doubling bifurcations [13]. During equibiaxial loading, the change occurs as transition to a more energetically favorable morphology for the corresponding strain [19].

The effects of equibiaxial and uniaxial strains have been extensively studied in the past due to the relative ease of access to equipment/techniques. However, due to lack of appropriate biaxial tensile stages, the effect of sequential biaxial loading is not well understood. Past studies demonstrate that stepwise loading, i.e., loading along one axis followed by loading along the orthogonal axis, leads to preferential selection of the zigzag mode [26–28]. This suggests the dependence of morphology on loading path in addition to the magnitude and nature of the strains. However, this path-dependence hypothesis is experimentally unverifiable in the absence of tools to apply loads along different paths. In fact, a majority of the design space remains unexplored due to the lack of experimental tools. Herein, we present the design and fabrication of the 2D tensile stage that enables exploring this design space.

2.3 Functional Requirements for Tensile Stage

2.3.1 Stretching-Driven Requirements. The purpose of the mechanical stage is to implement a well-controlled uniaxial and biaxial stretching of PDMS films. A well-controlled stretching operation is one in which (i) loading conditions are close to the idealized uniaxial/biaxial loading conditions and (ii) stretch values are accurately controlled. Here, "close to ideal" and "accurate" are relative terms and scale with the desired precision and fabrication tolerance of the wrinkles. For example, herein, we have used the critical strain of 0.3% as a benchmark for precision of strain. Thus, the desired strain resolution is set to one-tenth of this value and the maximum tolerable orthogonal strain due to parasitic motion is set to 0.3%. This corresponds to a parasitic motion limit of 130 μm; below this limit, parasitic stretching would not lead to wrinkle formation along the direction that is orthogonal to the nominal stretch. Additionally, the functional requirement for range of motion is derived from the need for large strains that exceed the period-doubling transition strain of ~18–20%. These requirements are summarized in Table 1.

2.3.2 Process-Driven Requirements. In addition to motion-based requirements, the stage must also satisfy the functional requirements that would enable a successful integration with other steps of the fabrication process. These requirements are: (i) the device must be smaller than the vacuum chamber for plasma oxidation and (ii) one must be able to quickly and accurately register the stage to the vision system. The need for registration arises out of the need to perform in situ process monitoring of wrinkle formation during stretch release. As the stage must be moved into the plasma chamber between the stretching and stretch-release steps, accurate registration of the stage to the vision system is critical. The desired registration accuracy is determined by the size of the area imaged by the vision system. Here, this has been set to 25% of the image side length. This selection ensures that a point located within 25% of the edge of an image can be registered back without moving the camera during repeated registration operations.

3 Design and Fabrication of Stage

We have designed and fabricated a system that satisfies the functional requirements for performing and visualizing wrinkle

Table 1 Functional requirements for the tensile stage

Metric	Value
Strain resolution	0.03% or better
Maximum prestretch	25% or higher
Parasitic motion	130 μm or less
Accuracy of registration to vision system	30 μm or better
Device footprint	Smaller than cylinder of 122 mm diameter and 450 mm length

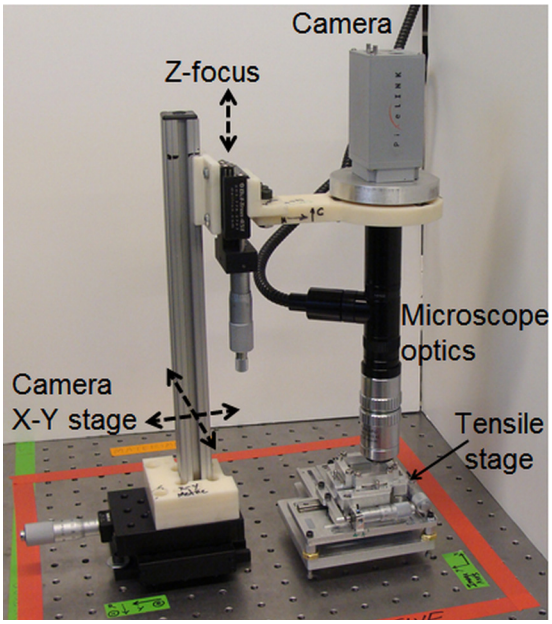

Fig. 3 Photograph of the designed system that consists of the tensile stage and the microscope stage. Holes on the table are on a 25.4 mm square spacing.

formation during uniaxial and biaxial stretch release. A photograph of the system is shown in Fig. 3. It consists of (i) a CMOS camera mounted on an X-Y-Z translation stage that forms the metrology frame and (ii) the biaxial tensile stage that is registered to the metrology frame. In this section, we link the functional requirements listed in Sec. 2.3 to design decisions and describe the design and fabrication of the modules of the tensile stage. Later in Sec. 4, we quantify the performance of the stage and evaluate its ability to satisfy the functional requirements.

To satisfy the functional requirements imposed by the wrinkling process, the following design parameters were selected: (i) the actuator should be integrated onto the stage to enable real-time tuning of wrinkles, (ii) nonessential motion guidance elements must be eliminated to reduce the size of the stage, and (iii) a mechanism for quick and accurate registration of the stage to the vision system must be implemented to enable in situ imaging. Herein, integrated onboard actuation was achieved by using manually actuated micrometer heads that were mounted on the stage. To reduce the size of the stage, mechanical couplings between the actuators and the movable platforms of the stage were eliminated; instead, the micrometer heads push directly onto the platforms during actuation. Additionally, a kinematic coupling was built into the base of the stage to quickly and accurately register the stage to the vision system.

3.1 Stage Modules. The biaxial stage may be functionally separated into distinct modules. These are: (i) fixtures to clamp and hold the PDMS film onto the stage, (ii) linear bearings for motion guidance, (iii) actuators for stretch/displacement control, (iv) base with kinematic coupling for registration, and (v) the structural frame. The purpose of the film clamping fixtures is to hold the edges of the PDMS film stationary along the actuated direction while allowing for motion along the orthogonal in-plane direction. To enable control of film stretch, the stage platforms are mounted on linear bearings and actuated individually and manually by micrometer heads. The purpose of kinematic couplings in the base is to implement an accurate and quick attach/detach mechanism to register the stage to the metrology frame. The purpose of the structural frame is to maintain structural rigidity and to provide alignment features for assembling the modules of the stage.

3.2 Fixturing of Films

3.2.1 PDMS Films. As the size of the motion stage scales with the size of the PDMS films being stretched, it is necessary to select the size of the PDMS films before designing the stage. The size of the films was determined by microfluidics-based applications, wherein the chip/device is about a centimeter to an inch square. For uniaxial stretching, we have used rectangular films, and for biaxial stretching, we have used symmetric cross-shaped films. The stretched length is 37.5 mm for rectangular films and 43 mm for cross-shaped films, clamped width is 20 mm, and the film thickness varies from 1.9 to 2.2 mm. The PDMS films were fabricated by thermally curing the commercially available Sylgard 184 two-part silicone elastomer mixture in a ratio of one part curing agent to 12 parts resin by weight. This generates PDMS films with a Young's modulus of 2.69 ± 0.03 MPa. Details of the curing protocol and measurement of Young's modulus are available elsewhere [29]. To align the edges of the film to the clamps, alignment features were generated on the bottom surface of the films by incorporating them directly into the molds used for curing. These alignment features ensure that the length of the stretched section is accurately known during stretching.

3.2.2 Film Clamping. The edges of the PDMS film are held onto the stage platforms via custom-made compression clamps that are illustrated in Fig. 4. These clamps were designed to provide a repeatable and sufficiently high compression during clamping. Each clamp consists of a set of two parts that when bolted together leave a fixed gap between the two. The gap between the two parts is designed to be smaller than the thickness of the PDMS films. Thus, when the PDMS film is clamped between these parts, the amount of clamping compression in the film is repeatable and is determined by the difference in the film thickness and the predetermined gap between the parts.

3.2.3 Avoiding Overconstraint. To avoid overconstraint during biaxial stretching, it is necessary to allow for the movement of the edges along the nonactuated direction. For example, edges oriented along the X direction must be free to move along the X axis whereas edges along the Y direction must be free to move along the Y axis. When all four edges are clamped, overconstraint can be avoided by implementing rolling boundary conditions at each edge. We have implemented these rolling edge conditions by introducing miniature linear ball bearings between each of the clamps bottoms and the corresponding platforms. The bearings are oriented along the edges, thereby allowing linear motion between the stage and the clamp along the edges as illustrated in Fig. 4. During biaxial loading, these roller bearings ensure that the stretches along the two axes are independent of each other.

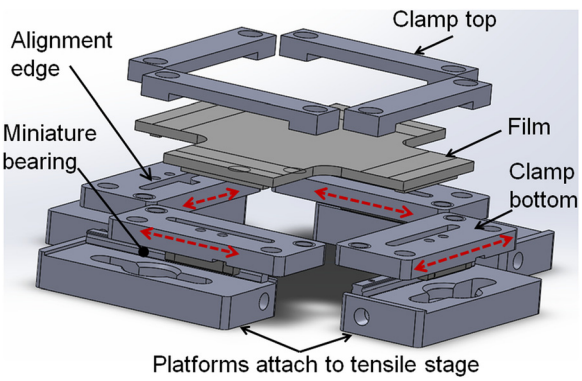

Fig. 4 Fixtures for clamping the PDMS films onto the tensile stage. Dashed arrows indicate the degree-of-freedom for clamp bottoms.

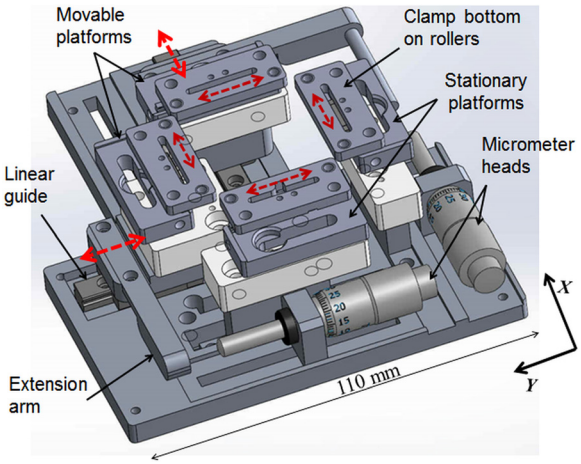

Fig. 5 Solid model rendering of the designed motion stage. Dashed arrows indicate the degree-of-freedom for the platforms and the clamps.

3.3 Motion Stage

3.3.1 Motion Guidance. The purpose of the motion stage is to provide the desired stretching motion while minimizing the parasitic motions. Based on the tradeoff for range versus accuracy, we selected linear bearings that are based on the ball guide and rail mechanism to guide motion along the two axes. This mechanism is illustrated in Fig. 5. The linear bearings for the two axes are oriented perpendicular to each other and can be independently actuated to stretch the PDMS film. To stretch the film, two orthogonal edges of the film are clamped onto stationary platforms and the corresponding opposing edges are clamped onto the moving platforms that are mounted on the linear guides. Actuation of each moving platform is performed manually via a micrometer head. As the two axes can be independently actuated, the stage may be used for both uniaxial and biaxial stretching.

3.3.2 Stage Actuation. We use micrometer heads that are mounted on the base of the stage to manually and independently actuate the two movable stages. To reduce the overall size and to integrate the heads onto the stage, mechanical couplings between the micrometer heads and the movable platforms were eliminated. Instead, the micrometer heads *push* directly onto the extension arms of the movable platforms. Each micrometer head sits in between the movable and stationary platforms and sets the *minimum distance* between the two platforms. As the heads are not rigidly connected to the movable platforms, they are incapable of pulling the platforms. Therefore, during actuation the movable platforms are free to move away from the stationary platforms, but not toward them. When PDMS films are mounted onto the stage and stretched, tension in the film provides the restoring force to the actuation motion. This restoring force on the movable platform keeps it from moving further away while the platform's position is held by the micrometer head. The PDMS film can be stretched further by actuating the micrometer to push onto the movable platform; whereas the tension can be released by actuating the micrometer in the opposite direction. Thus, actuation of the micrometer head can be used to control the tensile stretching of the PDMS film but cannot be used to compress it.

We have used the unidirectional actuation capability of the stage to accurately identify the zero stretch point during film stretching. During stretching and stretch release, the movable platform tracks the micrometer head and stays in contact with it as long as a nonzero restoring force due to tension exists. We measure this restoring force as the contact force between the micrometer head and the movable stage using a force-dependent resistor in half-bridge Wheatstone arrangement. The zero stretch point can then be identified within a tolerance band by measuring this contact force during stretching and stretch release. For the system designed here, the smallest force that could be accurately measured was 100 mN. This corresponds to an error of 0.06% in the film strain. This zero error is about two to five times less than the critical strain for wrinkling bifurcation and is substantially less than the operating strains of 5–15%.

3.3.3 Thermal Management. We have used passive thermal management schemes to ensure that mechanical stretching is minimally distorted by thermal strains and to hold positional accuracy during imaging. The film generation step that consists of plasma oxidation is the primary source of heat during the process. Thermal errors during film generation were managed by (i) performing intermittent plasma oxidation with a maximum continuous exposure time of 5 mins to prevent overheating of the stage and (ii) limiting the rise in temperature by increasing the thermal mass of the stage. The thermal mass of the stage was increased by attaching strips of a phase change material with a transition temperature of 50 °C on the exposed surfaces of the stage. These two schemes minimize the thermal errors associated with the film generation process. After film generation, the stage is cooled down to room temperature before performing any subsequent operation. This ensures that heating of the stage has minimal influence on position measurements during imaging.

The goal of thermal strain management was to maintain the residual thermal strain experienced by the stiff thin film lower than the critical wrinkling strain (ε_c); under this condition, thermal strains alone would not lead to wrinkled surfaces. Due to the layout of the mechanical constraints, there is no thermal strain in the PDMS film due to thermal expansion of PDMS. A stick figure model of the layout of the constraints in a single stretch axis is shown in Fig. 6. As the stiffness of PDMS is at least three orders of magnitude less than the stiffness of the base/micrometer, all of the thermal strain in PDMS is due to expansion of the micrometer head and the base of the stage. Thus, the thermal strain (ε_t) in the constrained PDMS film that arises due to a uniform temperature rise of ΔT is given by

$$\varepsilon_t = \Delta T\left(\frac{\alpha_b L_b + (L_s - L_b)\alpha_a}{L_s}\right) \tag{5}$$

Here, α_a and α_b are the coefficient of linear thermal expansion of the actuator and the base, L_s is length of the stretched PDMS film, and L_b is the distance between the base of the actuator and the fixed platform. The temperature rise necessary for a thermal strain that is equal to the critical strain can be estimated from the following values: $L_s = 43$ mm, $L_b = 18$ mm, $\alpha_a = 13 \times 10^{-6}$/K, $\alpha_b = 22.2 \times 10^{-6}$/K, and $\varepsilon_c = 0.1\%$. For these conditions, the maximum allowable rise in temperature of the stage is 59.3 °C.

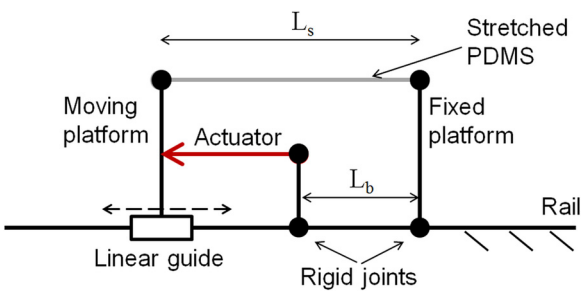

Fig. 6 Stick figure model depicting the layout of constraints for a single stretch axis. Circles represent rigid connectors. All straight lines, except the PDMS film, represent rigid members. The actuator is capable of only pushing onto the moving platform; it cannot pull the moving platform.

3.4 Vision System. We have assembled a custom microscope to satisfy the need for in situ visualization of wrinkle formation. The microscope consists of (i) optics for image magnification, (ii) an illuminator for coaxial illumination, (iii) a 5.0 MP CMOS camera (PixeLINK PL-B777U) to record the magnified image, and (iv) a manually actuated X-Y-Z stage to scan the sample surface and to focus the microscope. As this microscope uses reflected light instead of transmitted light for imaging, there are no components below the lens. This allows for the tensile stage to be freely positioned within the space below the microscope lens. The tensile stage was registered to the metrology frame by registering it to the fixed base of the X-Y-Z stage on the microscope. The microscope has a numerical aperture of 0.42, a working distance of 20 mm, a depth-of-field of 4 μm, and a lateral resolution of 0.86 μm. It enables recording grayscale reflected-light images of the wrinkled surface with a magnification of 35.1× and a captured area of 163 μm × 122 μm.

3.5 Registration of Stage to Vision System. We have used a "3-ball and V-groove" kinematic coupling to implement a quick and repeatable attach/detach mechanism for precise registration of the stage to the metrology frame. Kinematic couplings have been successfully used in the past to achieve registration with submicron repeatability for precision fixturing [30,31]. In this system, one-half of the coupling is aligned and rigidly attached to the metrology frame whereas the other half is aligned and attached to the stage. Preload to the coupling is provided by a pair of permanent magnets that are attached to the two-halves of the coupling. Thus, the stage can be registered to the vision system by engaging the two-halves of the coupling. Registration of the stage to the metrology frame involves aligning and locating the coordinate frames of the two systems with respect to each other. To enable quick registration, we perform alignment in two stages. First, we perform an initial alignment to *achieve* these registration requirements; then, we use the kinematic couplings to *maintain* the registration during repeated engagement–disengagement of the tensile stage from the metrology frame.

4 Performance of Stage

The performance of the tensile stage is summarized in Table 2. Herein, we (i) quantify the accuracy of the applied strain and the accuracy of registration and (ii) discuss the factors that affect the performance of the stage.

4.1 Accuracy of Strain

4.1.1 Mechanical Stretching. Accuracy of mechanical stretching is critical for an accurate control of the compressive strains in the film. Herein, we have measured and calibrated the displacement of the movable platforms during actuation. For calibration of each axis, a rectangular PDMS film was first mounted on the stage and then stretched by actuating the micrometer head; this was followed by reversing the direction of actuation to release the prestretch. The in-plane displacement of the movable stage was measured with a set of two Mitutoyo digital dial indicators (Digimatic Series 543) that had a resolution of 1 μm and an accuracy of ±3 μm. The indicators were aligned along and perpendicular to the direction of actuation. The results of these measurements are summarized in Fig. 7.

Under ideal conditions, the displacements of the platform and the actuator must be identical. However, the displacement of the platform was observed to be lower than that of the actuator because of the compliance in the parts between the platform and the actuator. This compliance was higher for the *Y* axis than the *X* axis due to a force sensor pad that was present on the *Y* axis but not on the *X* axis. Later in this work, the calibration curves generated in Fig. 7 have been used to correct for this reduction in strain due to machine compliance. The corresponding parasitic displacement of the stages along the in-plane orthogonal direction is limited to 56 μm for the *X* axis and 65 μm for the *Y* axis over a travel span of 5 mm. This verifies that the stage motion along the individual axis is indeed uniaxial over the travel distance.

4.1.2 Thermal Strains. The purpose of the passive thermal management scheme was to ensure that the thermal strains are smaller than the critical strain for wrinkling. To verify the effectiveness of this scheme, temperature at various spots on the stage was measured after an unstretched PDMS film was exposed to air plasma for 90 mins. The exposure cycle consisted of 5 mins of continuous exposure followed by a 5-min interval during which the plasma was switched off. Immediately after cumulative plasma exposure of 90 mins, temperature at various spots on the stage was measured using a thermocouple probe. The temperature was observed to vary within the range of 50–60 °C over the surface of the stage. The maximum temperature was observed on the clamps and the minimum temperature was observed on the exposed surface of the extension arm. The surface of the exposed PDMS film was examined under an atomic force microscope (AFM) to verify that no wrinkles were formed under thermal strains, i.e., the thermal strains were lower than the critical strain. Under the AFM microscope, a flat nonwrinkled surface was observed that had a surface roughness (Ra) of 3.5 nm over a scanned area of 30 μm × 30 μm. This justifies the approximation that the thermal strain on this tensile stage during plasma oxidation is negligible as compared to the strain due to mechanical stretching.

4.1.3 Stress Relaxation in PDMS. Due to the viscoelastic material behavior, the PDMS films exhibit stress relaxation. Thus, when the prestretch in a stretched PDMS film is released, the film does not fully recover back to its original position thereby leading to a residual stretch. This residual stretch in the PDMS base leads to a reduction in the compressive strain in the top film. In previous studies describing the wrinkling of mechanically stretched PDMS, this strain reduction has not been reported and/or accounted for. Although this phenomenon exists in such studies, its observation is hindered by the inability to detect the effect of stress relaxation in displacement-controlled actuation schemes. In such schemes, the PDMS film is "forced back" into the original position during prestretch release; in this position, the residual stretch in the base is often released via macroscale curvature of the bilayer. When such a bilayer is unclamped from the stage, the residual stretch

Table 2 Performance of the tensile stage

Metric	Value
Film unstretched length	37.5 mm (1D film) and 43 mm (2D film)
Displacement resolution	10 μm along each axis
Strain resolution	0.027% (1D film) and 0.023% (2D film)
Range of motion	13 mm along each axis
Parasitic motion	65 μm
Maximum prestretch, nominal	34.7% (1D film) and 30.2% (2D film)
Maximum prestretch, compliance corrected	33.5% (1D film), 29.2% along *X*, and 28.1% along *Y* (2D film)
Accuracy of registration to vision system	7 μm
Device footprint	131 mm × 110 mm × 75 mm

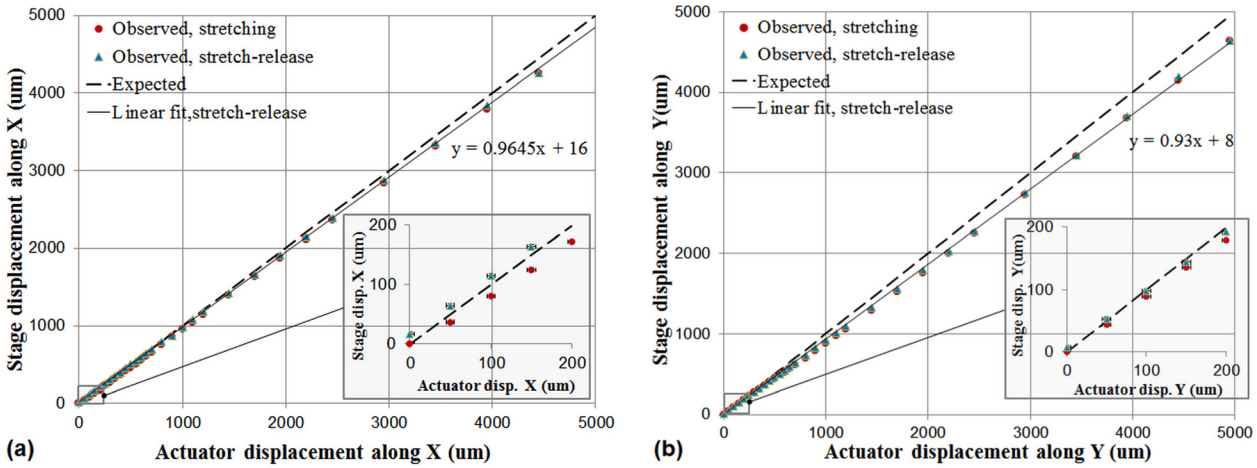

Fig. 7 Accuracy of mechanical stretching as quantified by the observed displacement of the stage versus the actuated displacement of the micrometer head for the (*a*) *X* axis and (*b*) *Y* axis. Insets are zoomed-out views close to the zero stretch point that illustrate the presence of residual stretch due to the stress relaxation effect.

persists in the base and leads to a reduction in the compressive strain in the top film.

In contrast, during prestretch release on this stage, the effect of stress relaxation can be distinctly observed from the premature loss of contact between the micrometer head and the stage arm. This is because the actuators on this stage can push but not pull onto the PDMS bilayers, i.e., compressive stretching is not feasible on this stage. The reduction in the film strain due to stress relaxation can be quantified by recording the position of the actuator at which it loses contact with the platform during prestretch release. Before this loss of contact, the compressive film strain increases with actuation of the micrometer head; after loss of contact, the strain does not increase with further actuation. The amount of stress relaxation is dependent on the time period over which the prestretch is held. The residual stretch due to stress relaxation over a time scale of 10 s can be observed during the stretch-release operation summarized in Fig. 7. During experiments with a cycle time of about an hour, a residual stretch of approximately 2% was observed for an initial prestretch of 15%. Later in this work, the strain reduction due to stress relaxation has been accounted for by recording the initial and final "zero-contact" positions.

4.2 Accuracy of Registration. Repeatability of the kinematic coupling is essential to maintaining the accuracy of registration between the stage and the microscope during repeated disengagement–engagement operations. Herein, we have measured the repeatability of the registration process by tracking the error in registration across multiple disengagement–engagement cycles. This was performed by tracking the in-plane displacement of two reference features on the surface of a PDMS film mounted on the stage. Each cycle was performed within 12 s while the stage was maintained at room temperature throughout the duration of the test. After each cycle, the position of the reference features was measured by capturing the image of the PDMS film with the microscope camera. Thus, this test captures the error in registration due to both (i) the kinematic coupling and (ii) the metrology frame.

The results of the repeatability test are summarized in Fig. 8. We observed that registration is repeatable to within 3 μm for the *X* axis and 7 μm for the *Y* axis. The larger error along the *Y* axis is due to the specific layout of the metrology frame. As the camera is mounted on a cantilever arm that extends along the *Y* axis, the stiffness of the *Y* axis is lower than the *X* axis. This difference in stiffness manifests as a larger error in registration along the *Y* axis. The observed error in the position of the features upon successive registration operations is at most 6% of the side length of the imaged surface. Thus, upon stage removal and re-engagement, one would be able to locate a preregistered feature on the surface without moving the camera. This ensures a quick and accurate registration during fabrication and tuning of wrinkles on this stage. To achieve this registration accuracy during operation, one must ensure that the temperature of the stage during successive registration events does not vary by more than 8 °C.

5 Fabrication and Tuning of Wrinkle Patterns

5.1 Uniformity of Patterning. Uniformity of patterning is a critical manufacturing metric that must be quantified when wrinkled patterns are desired over a large area. However, studies in the past have failed to quantify or characterize the uniformity of wrinkles. Lack of in situ metrology has been a major roadblock in characterizing uniformity. Here, we have used the in situ metrology system to quantify pattern uniformity by (i) mapping the spatial variation of period over the film surface and (ii) tracking the change in period with stretch release. These results are summarized in Fig. 9. The wrinkle patterns were obtained by releasing the stretch in a uniaxially prestretched PDMS film that was exposed to air plasma for 16 mins maintained at a power level of 250 W. Exposure of PDMS to air plasma generates a stiff thin glassy layer that has a Young's modulus of 3.20 ± 0.78 GPa. The

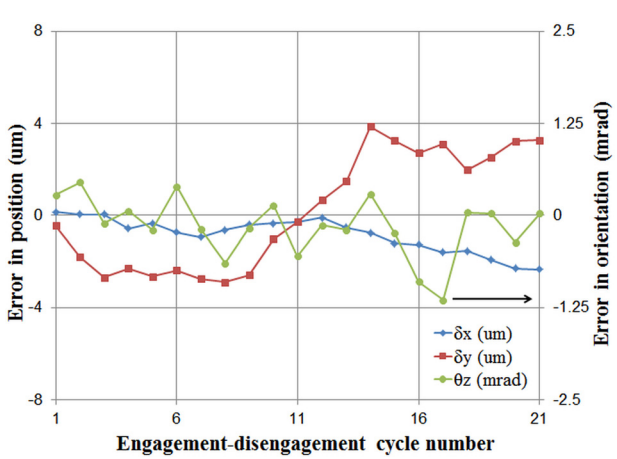

Fig. 8 Repeatability of registration between the stage and the vision system during successive engagement–disengagement cycles

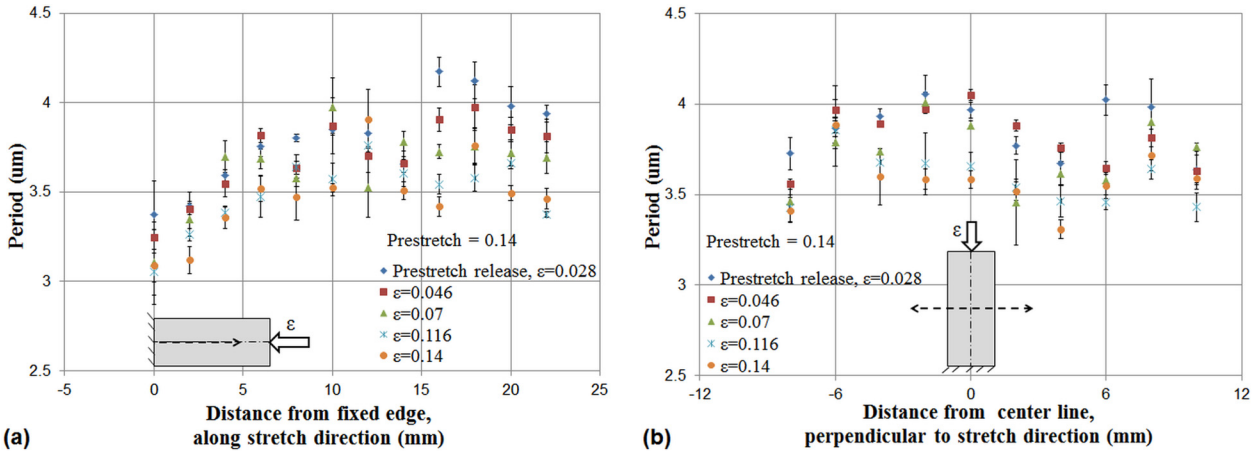

Fig. 9 Spatial variation in the period of wrinkles: (*a*) along the actuated direction and (*b*) orthogonal to the actuated direction. Error bars on period quantify the standard deviation of measurements over a single image frame that spans 163 μm × 122 μm.

calibration chart linking period to duration and power of plasma exposure and measurement of Young's modulus of the glassy layer is available elsewhere [29]. We observed that period varies with both the location of the measurement point and the amount of stretch released. Thus, the effect of these parameters must be accounted for and/or controlled during fabrication of wrinkled features over large areas.

With respect to the spatial variation of period, the edge effects manifest as a decrease in period in the vicinity of the edges. This variation is more prominent in the vicinity of the fixed edge, i.e., along the stretch direction. This is because of (i) the effect of the clamping action on the compressive strain and (ii) the shadowing effect of the clamps during plasma oxidation. At each stretch-release value, the spatial nonuniformity can be quantified by the variation in the period along the two axes. This nonuniformity in the period of the wrinkles is in the range of 5–6.5%.

With release of prestretch, one observes that the spatially averaged period decreases. This observation is not predicted by the linear elastic model represented in Eq. (1), which is based on the nondeforming coordinate system. As the experimental observation of period is based on the deformed configuration of the bilayer, one must use the deformed coordinate system to interpret these observations. On release of prestretch, the period decreases due to the compression of the deformed coordinate system. As this stretch-release effect is confounded by the effect of spatial variation, we have further studied this effect by tracking the evolution of period with stretch release at a single material point.

5.2 Stretch Release of 1D Patterns. During prestretch release, the period of wrinkles can be estimated by making the approximation that the number of wrinkles per unit undeformed length does not change. Thus, the observed period of the wrinkles in the deformed coordinates is related to the applied prestretch (ε_p) as

$$\lambda = \lambda_o \left(\frac{1 + \varepsilon_p - \varepsilon}{1 + \varepsilon_p - \varepsilon_o} \right) \tag{6}$$

Here, λ is the period at the current stretch, ε is the amount of stretch that has been released, and λ_o is the period when ε_o amount of stretch has been released. Prestretch and stretch release have the same unit as strain and are evaluated based on the initial undeformed length of the PDMS film. A positive stretch release corresponds to a state of compressive strain in the top film whereas a negative stretch release corresponds to a state of tensile strain.

The relationship in Eq. (6) was verified against experiments as shown in Fig. 10. These experiments were designed to minimize the effect of spatial nonuniformity in the measured period. This was achieved by moving the microscope along with stage actuation to ensure that the microscope tracks a material point on the wrinkled surface during prestretch release. The film was stretched by 14% prior to plasma oxidation. All models were calibrated to the experimental data point at the stretch-release value of 0.047. A rigorous model based on the finite deformation effect has been developed by Jiang et al. [21] that provides a marginal improvement in predictive accuracy with respect to our simplified model that is based on constant number of wrinkles. Hence, as a first approximation, Eq. (6) may be used to predict the change in period of the wrinkles as the prestretch in the base is released.

5.3 Higher 1D Mode. Complex higher mode wrinkles emerge from simple sinusoidal wrinkles when large compressive strains are applied to the bilayers. In the past, the phenomenon of period doubling at large strains has been experimentally demonstrated via direct compression of bilayers [13,24]. Although these studies provide valuable information about the period-doubling phenomenon, they are insufficient for predictive design and fabrication of period-doubled patterns. This is because replication/imprinting of the wrinkled patterns is practical only in prestretch-based film compression techniques.

As prestretch-based film compression and pure bilayer compression are not physically equivalent during large displacements [32], it is essential to separately characterize the prestretch-based technique. In the past, empirical studies of prestretch-based period doubling have been hindered by the absence of tools that can provide in situ imaging of wrinkle formation during prestretch release. In the absence of such tools, images of the wrinkled surface can be recorded only after the entire prestretch in the base is released. Thus, experiments that are performed to study the period-doubling phenomenon are limited to a binary outcome, i.e., presence or absence of period-doubled wrinkles on full prestretch release. Within this scheme, it is not possible to continually track the growth of sinusoidal wrinkles into higher modes with increase in the strain. Instead, a semicontinual scheme of applying varying prestretch levels to different bilayers must be employed. This introduces variability in the process and makes it difficult to accurately separate the effect of strain from other confounding variables such as variations in material properties and bilayer geometry. The tensile stage designed here overcomes this limitation by enabling in situ imaging of wrinkle formation. Herein, we demonstrate (i) the fabrication of period-doubled wrinkles of less than 5 μm period, i.e., period doubling on a length scale that has not been previously achieved in the PDMS/glassy film bilayer and (ii) the ability to accurately capture the mode

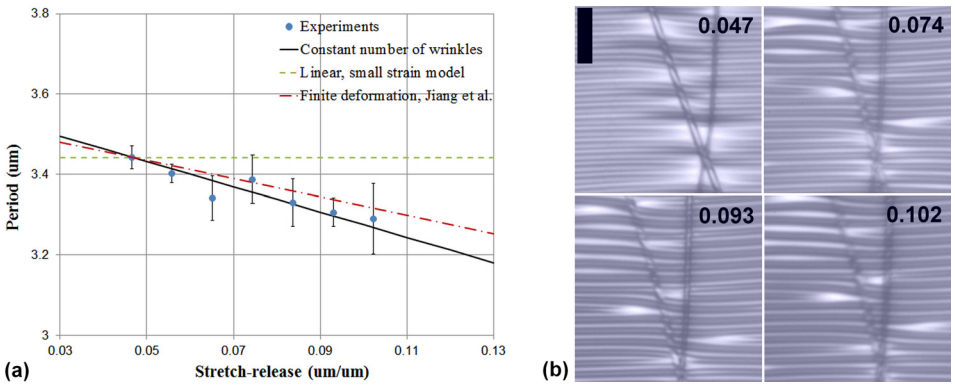

Fig. 10 (*a*) Effect of stretch release on the period of 1D wrinkles as measured by tracking a material point on a plasma-oxidized and uniaxially stretched PDMS film. (*b*) Close-up optical images of the defect zone that was tracked during experiments; scale bar is 15 μm long.

transition from sinusoidal wrinkles to period-doubled wrinkles by tracking the change in period of wrinkles during stretch release.

The change in the period of wrinkles during prestretch release was tracked by capturing the images of the wrinkled surface of a bilayer as the prestretch in it was released. The effect of stretch release on period is illustrated in Fig. 11. As the prestretch is released, one observes that (i) the period decreases up to a critical threshold strain, (ii) at the threshold, the wrinkles transition from the single-period sinusoidal mode into the period-doubled mode, and (iii) the period of the period-doubled mode decreases with further stretch release. In an optical image, the transition into period-doubled mode can be identified by the emergence of alternate bands of darker and lighter valleys that occur due to every alternate valley being shallower than its neighbor. Here, we observe that this transition occurs at a film compressive strain of 18.6%. Emergence of the period-doubled mode has also been verified with an AFM by capturing the profile of the wrinkled surface after full prestretch release. One such representative AFM profile of the period-doubled mode is shown in the inset of Fig. 11 that demonstrates the presence of shallower alternate valleys in the period-doubled mode.

As in situ imaging enables accurate measurements of the critical strain for mode transition, one may now use this measurement as an additional source of information for process

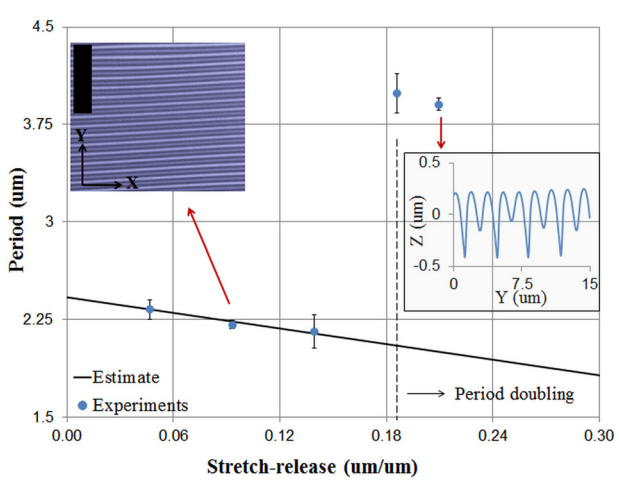

Fig. 11 Emergence of period-doubled mode at high compressive strains during stretch release of a plasma-oxidized and uniaxially stretched PDMS film. The film was stretched by 20.9% prior to plasma oxidation. Estimate is based on the approximation of constant number of wrinkles. Inset at the higher stretch-release is an AFM profile scan; inset at the lower stretch-release is an optical image, scale bar is 15 μm long.

calibration. For example, it is not feasible to separately estimate the material property ratio (η) and the film thickness (h) from measurements available from the single-period sinusoidal mode alone. This is because transition into the single-period mode from the flat state occurs at strains of 0.03–0.3% that are too low to reliably measure; thus, within this framework both the right-hand side and the left-hand side of Eq. (3) are unknown physical quantities. In contrast, the stage presented here can be used to separately estimate the parameters "η" and "h" by (i) measuring the critical strain for period doubling and (ii) linking the strain to η and h via physical relationships. In the absence of analytical models for the physical relationships, this stage may also be used to generate the appropriate empirical models.

5.4 Complex 2D Modes. A biaxial tensile stage enables fabrication and tuning of a variety of complex 2D wrinkle modes that are inaccessible via equibiaxial strains. With equibiaxial strains, one is limited to a small set of periodic 2D modes that consist of triangular, hexagonal, square checkerboard, and zigzag modes [22]. When equibiaxial compressive strain is generated via thermal expansion or volumetric swelling, these modes coexist over a surface such that no distinct mode can be deterministically obtained over the entire surface. Deterministic fabrication of the zigzag modes during mechanical stretch release has been demonstrated in the past via sequential release of stretch along one axis followed by release along the other axis [26–28]. These studies suggest that the formation of wrinkled patterns depends on both (i) the final biaxial strain and (ii) the loading path that generates the biaxial strain. Herein, we extend and generalize these techniques by independently actuating the two stages to generate unequal biaxial strains via a variety of different actuation paths.

We demonstrate the ability of our technique to generate patterns that are not accessible via equibiaxial strains by fabricating a nonuniform zigzag wrinkled pattern that exhibits period doubling only along one axis. Additionally, we demonstrate the feasibility of tuning patterns via tuning of (i) strain states and (ii) actuation paths. This was achieved by performing a series of biaxial stretch release and stretching operations on a bilayer film that consists of a titanium thin-film deposited on top of a biaxially prestretched PDMS film. The bilayer was fabricated by depositing a titanium film of thickness 84.2 ± 3.3 nm on top of a stretched PDMS film via RF sputtering. The PDMS base layer was prestretched by sequentially stretching the film along the Y axis by 6.0% and then along the X axis by 6.0%. During stretching along the Y axis, the X axis was held "free" to allow for Poisson's contraction along the X axis. Subsequent stretching along the X axis was performed from a starting position that corresponds to a zero normal stress along X. This stress state is ensured by the zero-contact condition of the actuation mechanism that is discussed in Sec. 3.3.2.

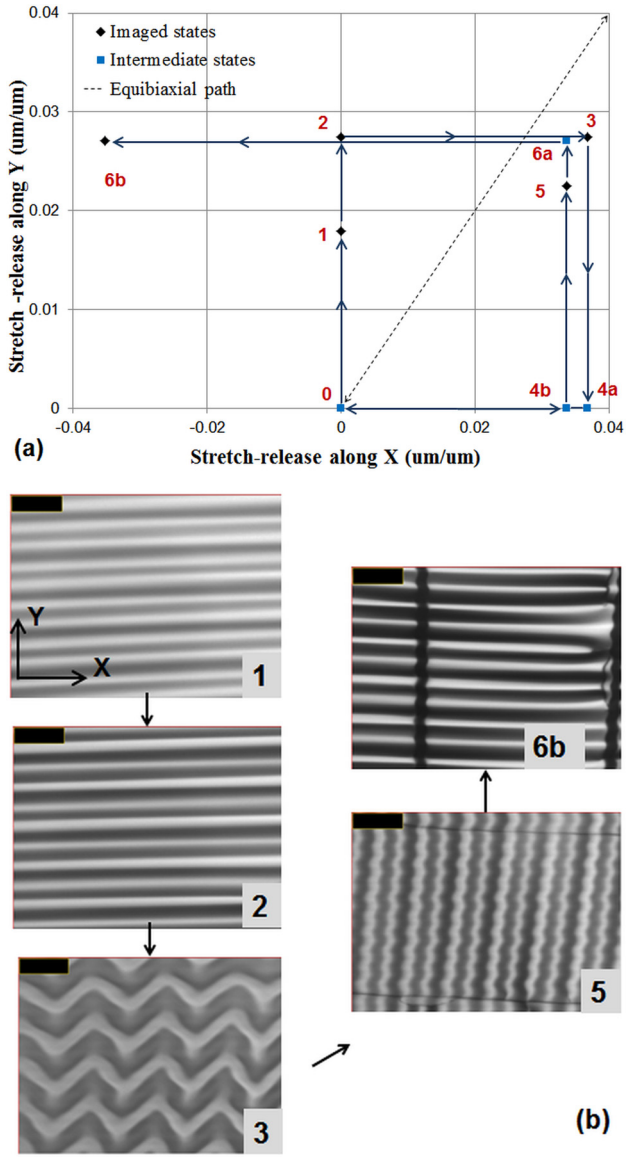

Fig. 12 Tuning of 2D wrinkle modes via biaxial strain state and strain history. (*a*) Strain states and history of strain. (*b*) Wrinkle mode shapes observed on a PDMS/titanium bilayer. Inset alphanumeric labels in the photographs correspond to labeled strain states along the actuation path. Scale bars are 30 μm long.

The sequence of stretch release and stretching operations is summarized in Fig. 12(*a*) and the corresponding patterns are shown in Fig. 12(*b*). Stretch release and stretching were performed along the following path: 0 → 1→ 2 → 3 → 4a → 0 → 4b → 5 → 6a → 6b. During uniaxial stretch release along *Y* axis from states 0 to 1, we observe the formation of 1D wrinkles that exhibit period-doubling behavior. Period doubling becomes more prominent with further stretch release from state 1 to state 2. On subsequent stretch release along the *X* axis, we observe the formation of zigzag patterns that demonstrate period doubling along both axes. The zigzag pattern is the characteristic pattern that is generated during sequential stretch release of a prestretched bilayer and is generated due to in-plane buckling of the aligned 1D wrinkles [26].

The patterns that are formed via wrinkling are reversible and can be tuned by changing the strain state and the actuation path. When the bilayer is stretched to bring it back from state 3 to a zero-strain state 0 via the intermediate state 4a, it is observed that the zigzag patterns transform into a flat state. Upon subsequent stretch release to state 5 via state 4b, a nonuniform zigzag pattern is obtained that has the dominant period oriented horizontally. The characteristics of this new asymmetric 2D pattern are: (i) smaller amplitude along the *Y* axis and (ii) period-doubling behavior along the *X* axis. This nonuniform zigzag pattern is formed due to the asymmetry in the *effective* compressive strains along the two axes. During the intermediate stretching and stretch-release steps, horizontally aligned cracks arise due to a mismatch between the Poisson's ratio of PDMS and titanium [7,33]. During stretch release along the *Y* axis, the effective compressive strain for buckling is reduced by the amount necessary for closing these cracks. This accounts for the lower amplitude along the *Y* axis of the zigzag patterns that are observed in state 5. Thus, this 2D tensile stage enables fabrication and tuning of such asymmetric 2D modes that are not accessible via equibiaxial strains.

Although the 2D patterns that are formed via wrinkling are actuation path dependent, they are not necessarily "locked-in." This means that the wrinkle pattern changes when the strain state is changed. Thus, it is possible to tune a wrinkled pattern across different modes by changing the strain states without ever going into an intermediate flat zero-strain state. Herein, we have demonstrated this tunability by changing the strain state of the bilayers from state 5 to state 6b via state 6a, as illustrated in Fig. 12(*b*). In the final state 6b, the titanium film is under tensile stretching along the *X* axis; this state of strain does not support wrinkle formation along the *X* axis. The observed wrinkled pattern in state 6b confirms this expectation as the pattern transforms from an asymmetric 2D mode into a uniaxial 1D mode that comprises horizontally aligned wrinkles. The tensile state of strain along the *X* axis can be verified by the presence of wide vertical cracks that are formed due to tensile stretching of the titanium film. These cracks can be further used to generate asymmetric 2D modes that are not accessible via equibiaxial strains.

6 Conclusions

We have designed a compact biaxial tensile stage that provides the means to apply accurate, large, and nonequal biaxial strains for wrinkle pattern formation. This stage can be used as (i) an experimental tool to study and characterize wrinkle formation and/or (ii) manufacturing equipment for low-cost fabrication of micro- and nano-scale patterns. Although the biaxial tensile stages that are capable of providing large and accurate strains are commercially available, adapting such stages for wrinkle pattern formation is challenging. These challenges arise due to the need for a mobile and compact stage that can (i) fit into vacuum chambers, (ii) accurately maintain the strain during thin-film generation/deposition, and (iii) readily allow for in situ imaging, i.e., real-time imaging during stretch release. We have solved these challenges by (i) eliminating mechanical coupling between the actuators and the movable platforms, (ii) integrating the actuators onto the stage, and (iii) incorporating a kinematic coupling to quickly and accurately register the stage to a custom-built vision system. The designed stage has a footprint of 131 mm × 110 mm × 75 mm and can provide a maximum strain of 33.5% with a resolution of 0.027% while holding an accuracy of 7 μm for repeated registrations to the vision system.

We have also demonstrated how one may apply this stage to study and characterize the wrinkling process. Specifically, we have demonstrated that (i) nonuniformity in the period of wrinkles over a plasma-exposed PDMS film is limited to 6.5%, (ii) single-period sinusoidal wrinkles of nominal period 2.3 μm transition into the period-doubled higher mode during prestretch release when the compressive strain exceeds around 18% for the PDMS/glassy film bilayer, and (iii) complex asymmetric 2D wrinkled patterns that are not accessible via equibiaxial strains can be fabricated via sequential unequal biaxial strains. Additionally, we demonstrate that the morphology of the 2D wrinkled pattern is determined by both the current strain state and the past strain history of the system. This strain path dependence of wrinkle pattern

formation opens up a new design scheme that enables one to reversibly and/or irreversibly reconfigure a single bilayer system to exhibit different types of wrinkled patterns. One may apply the stage developed here to systematically explore and characterize this design space to fabricate and tune reconfigurable 2D wrinkled patterns that are functionally relevant in applications such as optical and biological sensing.

Acknowledgment

S.K.S. would like to thank Mr. Aaron Ramirez and Dr. Isaac Ehrenberg at MIT LMP for their help with and access to RF sputterer for deposition of titanium thin films.

References

[1] Yin, J., Chen, X., and Sheinman, I., 2009, "Anisotropic Buckling Patterns in Spheroidal Film/Substrate Systems and Their Implications in Some Natural and Biological Systems," J. Mech. Phys. Solids, **57**(9), pp. 1470–1484.
[2] Wang, L., Castro, C. E., and Boyce, M. C., 2011, "Growth Strain-Induced Wrinkled Membrane Morphology of White Blood Cells," Soft Matter, **7**(24), pp. 11319–11324.
[3] Flynn, C. O., and McCormack, B. A. O., 2009, "A Three-Layer Model of Skin and Its Application in Simulating Wrinkling," Comput. Methods Biomech. Biomed. Eng., **12**(2), pp. 125–134.
[4] Genzer, J., and Groenewold, J., 2006, "Soft Matter With Hard Skin: From Skin Wrinkles to Templating and Material Characterization," Soft Matter, **2**(4), pp. 310–323.
[5] Mei, Y., Kiravittaya, S., Harazim, S., and Schmidt, O. G., 2010, "Principles and Applications of Micro and Nanoscale Wrinkles," Mater. Sci. Eng.: R, **70**(3–6), pp. 209–224.
[6] Stafford, C. M., Guo, S., Harrison, C., and Chiang, M. Y. M., 2005, "Combinatorial and High-Throughput Measurements of the Modulus of Thin Polymer Films," Rev. Sci. Instrum., **76**(6), p. 062207.
[7] Chung, J. Y., Lee, J.-H., Beers, K. L., and Stafford, C. M., 2011, "Stiffness, Strength, and Ductility of Nanoscale Thin Films and Membranes: A Combined Wrinkling-Cracking Methodology," Nano Lett., **11**(8), pp. 3361–3365.
[8] Khang, D.-Y., Rogers, J. A., and Lee, H. H., 2009, "Mechanical Buckling: Mechanics, Metrology, and Stretchable Electronics," Adv. Funct. Mater., **19**(10), pp. 1526–1536.
[9] Rogers, J. A., Someya, T., and Huang, Y., 2010, "Materials and Mechanics for Stretchable Electronics," Science, **327**(5973), pp. 1603–1607.
[10] Chung, S., Lee, J. H., Moon, M.-W., Han, J., and Kamm, R. D., 2008, "Non-Lithographic Wrinkle Nanochannels for Protein Preconcentration," Adv. Mater., **20**(16), pp. 3011–3016.
[11] Groenewold, J., 2001, "Wrinkling of Plates Coupled With Soft Elastic Media," Physica A, **298**(1–2), pp. 32–45.
[12] Chiche, A., Stafford, C. M., and Cabral, J. T., 2008, "Complex Micropatterning of Periodic Structures on Elastomeric Surfaces," Soft Matter, **4**(12), pp. 2360–2364.
[13] Brau, F., Vandeparre, H., Sabbah, A., Poulard, C., Boudaoud, A., and Damman, P., 2011, "Multiple-Length-Scale Elastic Instability Mimics Parametric Resonance of Nonlinear Oscillators," Nat. Phys., **7**(1), pp. 56–60.
[14] Bowden, N., Brittain, S., Evans, A. G., Hutchinson, J. W., and Whitesides, G. M., 1998, "Spontaneous Formation of Ordered Structures in Thin Films of Metals Supported on an Elastomeric Polymer," Nature, **393**(6681), pp. 146–149.
[15] Huck, W. T. S., Bowden, N., Onck, P., Pardoen, T., Hutchinson, J. W., and Whitesides, G. M., 2000, "Ordering of Spontaneously Formed Buckles on Planar Surfaces," Langmuir, **16**(7), pp. 3497–3501.
[16] Hobart, K., Kub, F., Fatemi, M., Twigg, M., Thompson, P., Kuan, T., and Inoki, C., 2000, "Compliant Substrates: A Comparative Study of the Relaxation Mechanisms of Strained Films Bonded to High and Low Viscosity Oxides," J. Electron. Mater., **29**(7), pp. 897–900.
[17] Huntington, M. D., Engel, C. J., Hryn, A. J., and Odom, T. W., 2013, "Polymer Nanowrinkles With Continuously Tunable Wavelengths," ACS Appl. Mater. Interfaces, **5**(13), pp. 6438–6442.
[18] Guvendiren, M., Yang, S., and Burdick, J. A., 2009, "Swelling-Induced Surface Patterns in Hydrogels With Gradient Crosslinking Density," Adv. Funct. Mater., **19**(19), pp. 3038–3045.
[19] Breid, D., and Crosby, A. J., 2011, "Effect of Stress State on Wrinkle Morphology," Soft Matter, **7**(9), pp. 4490–4496.
[20] Bowden, N., Huck, W. T. S., Paul, K. E., and Whitesides, G. M., 1999, "The Controlled Formation of Ordered, Sinusoidal Structures by Plasma Oxidation of an Elastomeric Polymer," Appl. Phys. Lett., **75**(17), pp. 2557–2559.
[21] Jiang, H., Khang, D.-Y., Song, J., Sun, Y., Huang, Y., and Rogers, J. A., 2007, "Finite Deformation Mechanics in Buckled Thin Films on Compliant Supports," Proc. Natl. Acad. Sci., **104**(40), pp. 15607–15612.
[22] Cai, S., Breid, D., Crosby, A. J., Suo, Z., and Hutchinson, J. W., 2011, "Periodic Patterns and Energy States of Buckled Films on Compliant Substrates," J. Mech. Phys. Solids, **59**(5), pp. 1094–1114.
[23] Hutchinson, J. W., 2013, "The Role of Nonlinear Substrate Elasticity in the Wrinkling of Thin Films," Philos. Trans. R. Soc., A, **371**(1993).
[24] Sun, J. Y., Xia, S., Moon, M. W., Oh, K. H., and Kim, K. S., 2011, "Folding Wrinkles of a Thin Stiff Layer on a Soft Substrate," Proc. R. Soc. A, **468**(2140), pp. 932–953.
[25] Wu, D., Yin, Y., Xie, H., Shang, Y., Li, C., Wu, L., and Dai, X., 2014, "Controlling the Surface Buckling Wrinkles by Patterning the Material System of Hard-Nano-Film/Soft-Matter-Substrate," Sci. China: Phys., Mech. Astron., **57**(4), pp. 637–643.
[26] Yin, J., Yagüe, J. L., Eggenspieler, D., Gleason, K. K., and Boyce, M. C., 2012, "Deterministic Order in Surface Micro-Topologies Through Sequential Wrinkling," Adv. Mater., **24**(40), pp. 5441–5446.
[27] Yin, J., Yague, J. L., Boyce, M. C., and Gleason, K. K., 2014, "Biaxially Mechanical Tuning of 2-D Reversible and Irreversible Surface Topologies Through Simultaneous and Sequential Wrinkling," ACS Appl. Mater. Interfaces, **6**(4), pp. 2850–2857.
[28] Lin, P. C., and Yang, S., 2007, "Spontaneous Formation of One-Dimensional Ripples in Transit to Highly Ordered Two-Dimensional Herringbone Structures Through Sequential and Unequal Biaxial Mechanical Stretching," Appl. Phys. Lett., **90**(24), p. 241903.
[29] Saha, S. K., 2014, "Predictive Design and Fabrication of Complex Micro and Nano Patterns Via Wrinkling for Scalable and Affordable Manufacturing," Ph.D. thesis, Massachusetts Institute of Technology, Cambridge, MA, http://hdl.handle.net/1721.1/93860.
[30] Slocum, A. H., 1988, "Kinematic Couplings for Precision Fixturing—Part I: Formulation of Design Parameters," Precis. Eng., **10**(2), pp. 85–91.
[31] Schouten, C. H., Rosielle, P. C. J. N., and Schellekens, P. H. J., 1997, "Design of a Kinematic Coupling for Precision Applications," Precis. Eng., **20**(1), pp. 46–52.
[32] Cao, Y., and Hutchinson, J. W., 2012, "Wrinkling Phenomena in Neo-Hookean Film/Substrate Bilayers," ASME J. Appl. Mech., **79**(3), p. 031019.
[33] Saha, S. K., and Culpepper, M. L., 2012, "Predicting the Quality of One-Dimensional Periodic Micro and Nano Structures Fabricated Via Wrinkling," ASME Paper No. IMECE2012-87081.